Properties and Structural Characterization of Oxidized Starch/PVA/α-Zirconium Phosphate Composites

Yajuan Yang,[1] Changhua Liu,[1] Peter R. Chang,[2,3] Yun Chen,[2,4] Debbie P. Anderson,[2] Mark Stumborg[2]

[1]*College of Chemistry and Chemical Engineering, Southwest University, Chongqing 400715, China*
[2]*Biobased Platforms, Agriculture and Agri-Food Canada, 107 Science Place, Saskatoon S7N 0X2, SK, Canada*
[3]*Department of Agricultural and Bioresource Engineering, University of Saskatchewan, Saskatoon S7N 5A9, SK, Canada*
[4]*Department of Biomedical Engineering, School of Basic Medical Science, Wuhan University, Wuhan 430071, China*

Received 29 April 2009; accepted 10 July 2009
DOI 10.1002/app.31099
Published online 15 September 2009 in Wiley InterScience (www.interscience.wiley.com).

ABSTRACT: Two series of composites, i.e., polyvinyl alcohol (PVA)/oxidized starch (OST)/exfoliated α-zirconium phosphate (POST-ZrPn) and PVA/starch (ST)/exfoliated α-zirconium phosphate (PST-ZrPn), were fabricated using a casting and solvent evaporation method. The composites were characterized by Fourier transform infrared spectroscopy (FT-IR), thermal gravimetric analysis (TGA), differential scanning calorimetry (DSC), wide-angle X-ray diffraction (XRD), scanning electron microscopy (SEM), tensile testing, and moisture uptake. Compared with PST-ZrPn, POST-ZrPn films with the same component ratio showed higher tensile strength (σ_b), lower elongation at break (ε_b) and improved water resistance. Additionally, in the POST-ZrPn series, σ_b and ε_b increased with an increase in α-zirconium phosphate (α-ZrP) loading; however, higher α-ZrP loads resulted in the aggregation of α-ZrP particles. Compared with POST-ZrP0, the values for σ_b, ε_b, and water resistance of POST-ZrP3, containing 1.5 wt % α-ZrP, were increased by 128.8%, 51.4%, and 30.2%, respectively. © 2009 Wiley Periodicals, Inc. J Appl Polym Sci 115: 1089–1097, 2010

Key words: composites; nanocomposites; structural-property relations; thermal properties; thermogravimetric analysis (TGA)

INTRODUCTION

Natural polymers from renewable resources have been considered to be excellent raw materials for replacement of petroleum resources.[1–3] Because of its abundant supply, low-cost, good processability, biodegradability, and ease of physical and chemical modification, starch (ST) has been considered one of the most promising raw materials and, as a consequence, has been used in various fields in degradable plastics, and in blend films in the agriculture, medicine, and packaging industries.[4] There are some limitations in developing ST-based products because of poor mechanical properties and high moisture sensitivity.[5] In this regard, blending ST with synthetic polymeric materials seems quite prudent. In fact, ST/PVA has been investigated as a potential biodegradable polymer in several studies[6–11]; however, because ST is only partially compatible with PVA, the tensile strength and elongation at break of the ST/PVA composites were not significantly improved. On the other hand, polymer/natural montmorillonite (MMT) composites exhibit improved physical and mechanical properties.[12–15] α-Zirconium phosphate (α-ZrP) exhibits great advantages over MMT clay, including a much higher purity and surface energy, ease of intercalation, and ease of exfoliation.[16] Moreover, the particle size and aspect ratio of α-ZrP can be manipulated by varying the reaction conditions.[17] The application of α-ZrP as nanofiller in polymer matrices for preparing nanocomposites has been reported recently.[18–20] Such nanocomposites not only exhibit excellent mechanical and barrier properties, but also possess improved thermal stability.

Oxidized starch (OST) obtained after treatment with potassium permanganate was used in this study. α-ZrP with a large interlayer spacing was used to fabricate PVA/ST/α-ZrP and PVA/OST/α-ZrP nanocomposites. It is hypothesized that the newly introduced carboxyl groups in ST after oxidation will improve compatibility between OST and PVA molecules. The structure and properties of

Correspondence to: P. R. Chang (peter.chang@agr.gc.ca).
Contract grant sponsor: The Program of Energy Research and Development (PERD) of Natural Resources Canada and the Pulse Research Network (PURENet), through Agriculture and Agri-Food Canada's Agriculture Bioproducts Innovation Program (ABIP).

TABLE I
Code for POST-ZrPn and PST-ZrPn Nanocomposite Films

Series #1[a]	OST or ST (g)	PVA (g)	Glycerol (g)	α-ZrP (g)	Water (mL)	Series #2[a]
OST-0	2	0	0.6	0	80	ST-0
POST-ZrP0	2	0.5	0.6	0	80	PST-ZrP0
POST-ZrP1	2	0.5	0.6	0.01	80	PST-ZrP1
POST-ZrP2	2	0.5	0.6	0.02	80	PST-ZrP2
POST-ZrP3	2	0.5	0.6	0.03	80	PST-ZrP3
POST-ZrP4	2	0.5	0.6	0.04	80	PST-ZrP4
POST-ZrP5	2	0.5	0.6	0.05	80	PST-ZrP5
POST-ZrP6	2	0.5	0.6	0.06	80	PST-ZrP6

[a] Series #1 corresponds to OST-based series; and series #2 corresponds to ST-based series.

the PVA/ST/α-ZrP and PVA/OST/α-ZrP nanocomposites were comparatively studied. The effect of α-ZrP content on the performances of these two series nanocomposite films was also investigated.

EXPERIMENTAL

Materials

Field pea starch, with an average granule size of 29 μm and composed of 35% amylose and 65% amylopectin, was supplied by Nutri-Pea Limited Canada (Portage la Prairie, Canada). Glycerol (99% purity), polyvinyl alcohol (PVA) (DP 1788 ± 50), potassium permanganate (analytical grade), and sulfuric acid were from Maoye Chemical Company (Chongqing, China). $ZrOCl_2 \cdot 8H_2O$ (99% purity) was purchased from Tianjin Kermel Chemical Reagent Development Center (Tianjin, China). *n*-Butylamine (99% purity) was obtained from Chengdu Kelong Chemical Reagent Company (Chengdu, China).

Preparation of OST and determination of degree of oxidation

OST was prepared using the following method[21]: A 40 wt % (w/w) starch slurry (total weight 175 g) was stirred in a water bath. When the slurry temperature reached 50°C, 2.5 mL of 3 MH_2SO_4 and 12.5 mL of 2% $KMnO_4$ were added. The mixture was then stirred at the same temperature until the color changed to milky white (about 2 h). The OST was filtered and washed 10 times with distilled water, and then air-dried at 40°C for 48 h. The carboxyl content (determination of degree of oxidation) of the resulting OST was determined according to the procedure of Chattopadhyay et al.[22] and was calculated to be 0.0945%.

Synthesis and exfoliation of α-ZrP

α-ZrP was synthesized according to a previous study.[23] The α-ZrP was intercalated by the following method: α-ZrP powder was dispersed in deionized water with a liquid-solid ratio of 100 mL/g. *n*-Butylamine was added to the mixture and the controlled molar ratio of amine and α-ZrP was 2.5. The α-ZrP suspension was treated by ultrasonication over night.[24]

Preparation of the POST-ZrPn and PST-ZrPn films

The glycerol-plasticized POST-ZrPn films were fabricated by a casting and solvent evaporation method. The PVA/OST solution was prepared by dissolving 2 g OST and 0.5 g PVA in 80 mL water with 30 wt % (based on OST) glycerol. The suspension was stirred at 95°C for 30 min until the solution became transparent and starch paste was obtained. The exfoliated α-ZrP (varying from 0 to 3 wt % of OST) was then added and the mixture stirred for another 30 min at 65°C and then coded as POST-ZrPn (where *n* is the percent of α-ZrP on OST). After degassing under vacuum, the composite was cast into a plexiglass plate placed on a flat, level surface and dried in an oven at 45°C for 12 h. The completely dried films were then peeled off of the plexiglass plate. To serve as experimental controls, the neat starch film (ST-0), the neat OST film (OST-0), and the PVA/ST/α-ZrP blend films (PST-ZrPn), were obtained through the same fabrication process. The codes for all films are listed in Table I. The resulting films were kept at room temperature in a conditioning desiccator at 43% relative humidity (RH) for more than 1 week to ensure equilibrium of water in the films prior to characterization.

Characterization of the composite films

Fourier transform infrared spectroscopy

Fourier transform infrared (FT-IR) spectra of the blend films were recorded with a Nicolet (Madison, WI) 170SX FT-IR spectrometer in the attenuated total reflection mode, wavelength range 4000–650 cm^{-1}.

The X-ray diffractometry

X-ray diffractometry was performed on an XRD-3D, PuXi, (Beijing) X-ray diffractometer with nickel filtered Cu Kα radiation (λ = 0.15406 nm) at a current of 20 mA and a voltage of 36 kV. The scanning rate was 4°/min in the angular ranges of 3–30° and 3–40° (2θ).

Scanning electron microscopy (SEM)

A scanning electron microscope (S-4800, HITACHI, Japan) was used to observe the morphologies of sample cross-sections at an accelerating voltage of 5 kV. Blend films from the two series containing different α-ZrP levels were fractured in liquid nitrogen, the cross-sections mounted on SEM stubs with double-sided adhesive tape, and then coated with gold in a 13.3 Pa vacuum.

Thermal analyses

Thermal gravimetric analysis (TGA) of the blend films was carried out on a TA-STDQ600 (TA Instruments, New Castle, DE). The thermograms were acquired between 25 and 500°C at a heating rate of 10°C/min. Nitrogen was used as the purge gas at a flow rate of 20 mL/min. An empty pan was used as a reference. Differential scanning calorimetry (DSC) measurements of the nanocomposites were performed under a nitrogen atmosphere on a NETZSCH DSC 200 F3 instrument in the temperature range of 25 to 250°C with a heating rate of 20°C /min. Aluminum pans containing 2 to 3 mg of film were sealed with a pierced lid using the DSC sample press. All samples were preheated over a temperature range of 25–100°C, held at 100°C for 10 min to remove the residual water, cooled to 25°C, and then heated to 250°C.

Mechanical properties

The tensile strength and elongation at break of the blend films were tested using a Universal Testing Instrument Model Sans 6500 (Shenzhen Sans Test Machine Co., Shenzhen, China) according to the Chinese standard method (GB 13,022-91). All films were cut into 10 × 100 mm long strips and mounted between cardboard grips (150 × 300 mm) using adhesive so that the final area exposed was 10 × 50 mm. The cross-head speed was 10 mm/min. All film measurements were performed on three specimens and averaged.

Moisture uptake test

The moisture uptake (MU) of the POST-ZrPn and PST-ZrPn blend films was determined by following the method of Mathew et al.[25] The samples used were thin rectangular strips with dimensions of 50 mm × 10 mm × 0.1 mm. They were vacuum dried overnight at 80°C and then kept at 0% RH (P_2O_5) for 1 week. After weighing, they were conditioned at room temperature in a desiccator of 92% RH (Na_2CO_3 saturated solution). The MU of the samples was calculated as follows:

$$\mathrm{MU} = (W_1 - W_0)/W_0 \times 100\%$$

where W_0 and W_1 were the weights of the sample before exposure to atmosphere and after equilibrium, respectively. An average value of three replicates for each sample was taken.

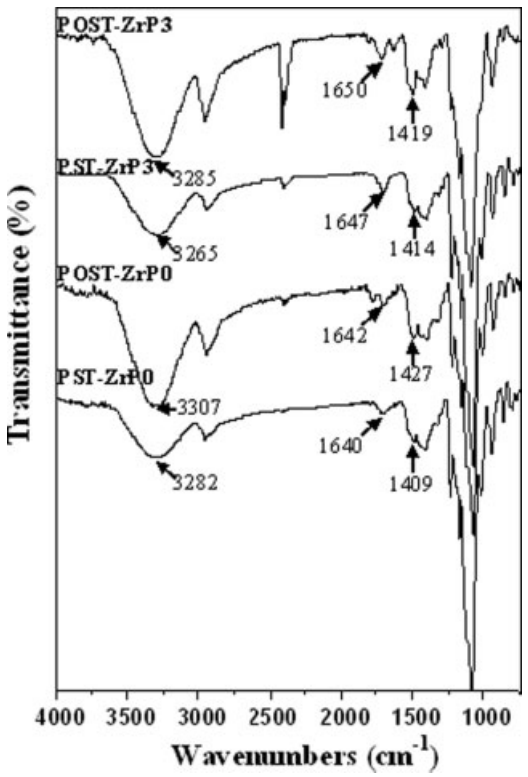

Figure 1 FT-IR spectra of PST-ZrP0, PST-ZrP3, POST-ZrP0, and POST-ZrP3.

RESULTS AND DISCUSSION

FT-IR analysis

The FT-IR spectra of selected films are shown in Figure 1. In the spectrum for PST-ZrP0, the stretching and bending vibration of the hydrogen bonding —OH group occurred at 3282 and 1640 cm^{-1}, respectively. The bands at 1150 cm^{-1} and 1078 cm^{-1} were attributed to the stretching vibration of C—O in the C—O—H groups, and the band at 994 cm^{-1} was attributed to the stretching vibration of C—O in the C—O—C groups. The characteristic peak of the C—O—C ring vibration in starch is located at

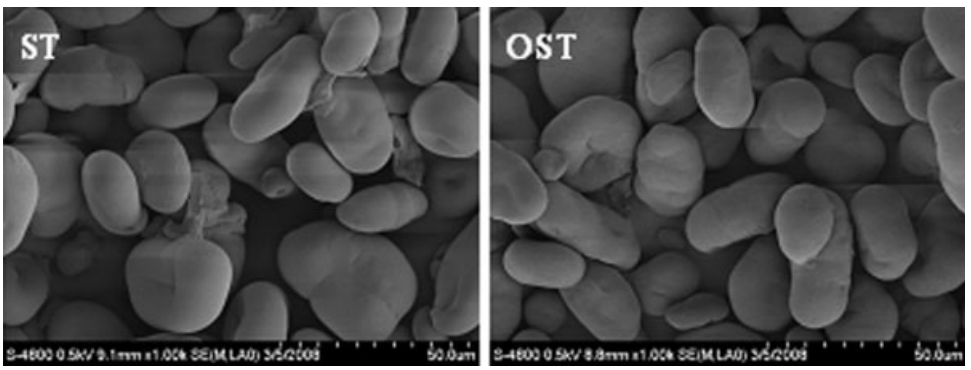

Figure 2 SEM images for ST and OST powder.

761 cm^{-1}. The bands attributed to the CH and CH_2 deformation vibrations were present in the 1300–1500 cm^{-1} range. As with almost all organic compounds, an absorption band because of the stretching vibrations of the CH and CH_2 groups could be seen at 2925 cm^{-1}.[26]

Compared with PST-ZrP0, POST-ZrP0 had a new peak at 1723 cm^{-1}, which was attributed to the C=O stretching vibration. This indicated that the hydroxyl groups in the C-6 positions of ST were oxidized and that the carboxyl groups had been introduced.[21] Additionally, the peaks at 3282 cm^{-1} for —OH groups in PST-ZrP0 shifted to 3307 cm^{-1} in POST-ZrP0. This change indicated that the carboxyl groups introduced to starch molecules also formed hydrogen bonding interactions with the —OH groups in PVA. In PST-ZrP0, the hydrogen bonding interactions mainly occurred between —OH and —OH; however, in the POST-ZrP0, the hydrogen interactions were enhanced in the presence of carboxyl, which possessed stronger polarity. The binding constant of hydrogen bonding between PVA and OST, therefore, increased and the peak moved toward a higher wavenumber.

In the FT-IR spectra for PST-ZrP3 and POST-ZrP3, the absorption peaks for —OH were at 3265 and 3285 cm^{-1}, respectively, 17 and 22 cm^{-1} lower than those of PST-ZrP0 and POST-ZrP0. α-ZrP interacted with matrix, and partially destructed the hydrogen bonding between PVA and ST (or OST). As a result, the absorptions of —OH groups shifted to lower wavenumbers. However, the peak corresponding to —OH groups in POST-ZrP3 (3285 cm^{-1}) was higher that in PST-ZrP3 (3265 cm^{-1}), indicating that the hydrogen bonds in POST-ZrP3 were stronger than those in PST-ZrP3 because of the existence of polar carboxyl groups in POST.

Scanning electron microscopy

Scanning electron micrographs revealed that both native and oxidized field pea starch granules were oval or spherical in shape and 20–40 μm in diameter. The SEM photographs of the ST and OST powders are shown in Figure 2. No obvious differences were observed on the surface of the ST granules after oxidation. This is the same as that of hypochlorite oxidized field pea starch reported by Li and Vasanthan.[27] Morphological images of select nanocomposite films and α-ZrP are shown in Figure 3. The α-ZrP showed a plate-like structure and regular cubic sheets, indicating that its crystallinity was very high, which was also proven by XRD (Fig. 4(I)). It was observed that the cross-section of the PST-ZrP0 film was very rough, an indication that the adhesion or compatibility between ST and PVA was quite poor, leading to phase separation of the two polymers. The cross-section of the POST-ZrP0 composite film was much smoother than that of PST-ZrP0. The fine, homogenous dispersion of PVA in the OST matrix can be seen in the image. Similar phenomena were also observed in PST-ZrP3 and POST-ZrP3 indicating that the interfacial adhesion and compatibility of blend samples containing OST were significantly improved. Moreover, PST-ZrP3 showed that even with a small addition of exfoliated α-ZrP (1.5 wt %), the interface between PVA and ST became flat, and the phase size was reduced. The cross-sections of POST-ZrP3 appear much smoother than the other nanocomposite films (POST-ZrP1 or POST-ZrP6), indicating that α-ZrP formed a stronger interaction with the polymers and dispersed more homogenously in the matrix, resulting in the best mechanical properties (discussed in Mechanical properties section). Higher loading of α-ZrP may result in aggregation of α-ZrP particles, as shown with arrows in the cross-section SEM image of POST-ZrP6 film, which indicates a certain degree of phase separation between α-ZrP and PVA/OST. This could explain why the mechanical properties became worse when the α-ZrP content was 3 wt %.

XRD analysis

The XRD patterns of the original materials and resulting films are shown in Figure 4. In Figure 4(I),

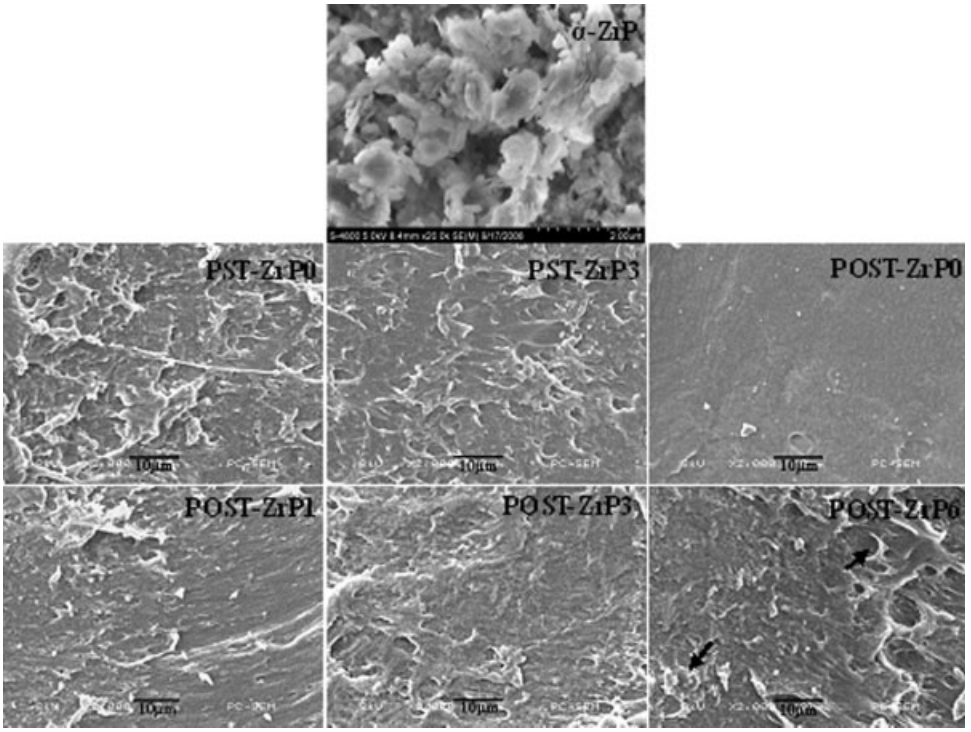

Figure 3 SEM images for select POST-ZrPn and PST-ZrPn films, arrows in POST-ZrP6 indicate aggregated α-ZrP.

the first peak of α-ZrP (curve "a") indicates (001) reflections of α-ZrP. The interlayer distance in the (001) direction was estimated from Bragg's law, $2d\sin\theta = \lambda$. The first peak of exfoliated α-ZrP (curve "b") shifted to a lower angle, corresponding with the lattice expansion from 7.4 Å to 16.8 Å because of the intercalation of amine. This can be taken as evidence of α-ZrP being intercalated and exfoliated.[28]

In Figure 4(II), for ST-0, the typical C-type crystalline pattern, with peaks at $2\theta = 5.7°$ (characteristic of B type polymorphs), 15.1° (characteristic of A type polymorphs), 17.21° (characteristic of both A and B type polymorphs), 20.18° and 22.58° (characteristic of B type polymorphs), was observed clearly.[29] Following the oxidation treatment, OST-0, there were no obvious changes in the diffraction pattern, indicating that the crystalline structure for starch was not affected by the oxidation reaction. PVA showed an obvious diffraction peak at $2\theta = 19.28°$.[30] This peak may be attributed to the strong intermolecular interaction between PVA chains through the intermolecular hydrogen bond.[31]

Fig. 4(III) shows the XRD patterns of PST-ZrP0 and POST-ZrPn nanocomposites with various exfoliated α-ZrP loading. Compared with PST-ZrP0, the pattern for POST-ZrP0 shows an amorphous hill accompanied by slightly weaker crystalline peaks, indicating a higher ratio of amorphous structure and lower crystallization. This also proves that the stronger hydrogen bonding between OST and PVA chains effectively prevented regular packing of the

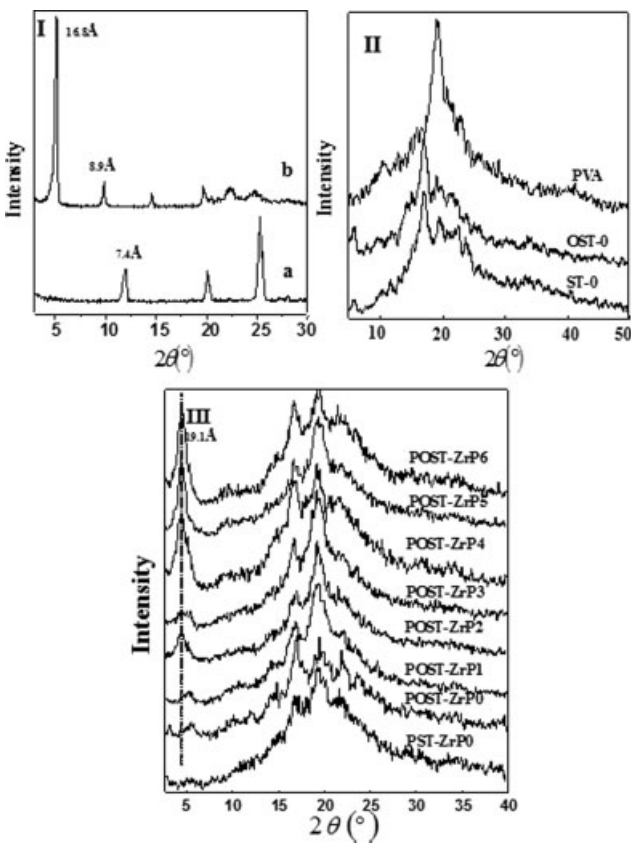

Figure 4 XRD patterns of original materials and POST-ZrPn nanocomposite films.

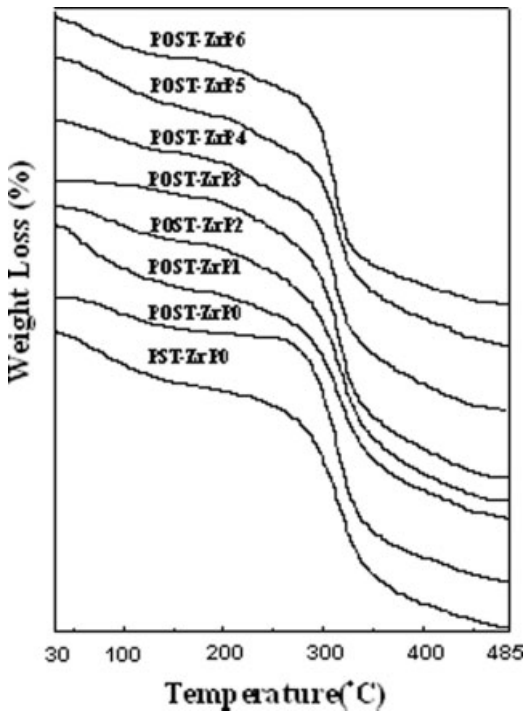

Figure 5 TGA curves for PST-ZrP0 and POST-ZrPn nanocomposite films with different α-ZrP contents.

modified starch. Additionally, it was worth noting the difference among POST-ZrPn nanocomposites. In Figure 4(I), exfoliated α-ZrP shows a sharp (001) diffraction at $2\theta = 5°$ corresponding to a d-spacing of 1.68 nm. However, after compounding with PVA and OST, this peak shifted slightly to $2\theta = 4.6°$ (d-spacing = 1.91 nm) (Fig. 4 (III)). This indicated that PVA or OST molecules intercalated into the α-ZrP layer and further expanded the spacing of α-ZrP not only because of the higher d-spacing of α-ZrP but also because of the improved interface compatibility between OST, PVA, and α-ZrP. The presence of the $2\theta = 4.6$ peak shows that some α-ZrP aggregated during processing. The intensity of this peak increased with an increase in α-ZrP loading but decreased sharply in POST-ZrP3 indicating that in the POST-ZrP3 blend film, the α-ZrP dispersed more homogenously in the PVA/OST matrix than it did in other films. Moreover, the XRD intensities of the POST-ZrPn nanocomposites increased with the increase in α-ZrP loading, indicating an enhanced crystallization ability of the POST-ZrPn blend in the presence of nanofillers, which may behave as nucleating agents.

Thermogravimetric and differential scanning calorimetry analyses

Figures 5 and 6 show the TGA and DTG thermographs of PST-ZrP0 and POST-ZrPn nanocomposites. The TGA and DTG curves of all polymer films revealed three main weight loss regions, which appeared as three peaks in the DTG curves. The first region at 80–115°C was due to the removal of water; the second transition region at 250–350°C was due to degradation of the polymer films; and the peak of the third stage, at 425°C, was due to cleavage of the polymeric backbone.[32] Compared with POST-ZrP0, the thermal degradation temperature shifted about 5°C higher for the composite with 1.5 wt % α-ZrP.

DSC curves for POST-ZrPn nanocomposites are shown in Figure 7. All nanocomposites were found to have higher T_g values than POST-ZrP0, as shown in Table II. This indicates that the α-ZrP nanoparticles, which appended on the main chain prevented the segmental motion of polymer chains. Additionally, with an increase in α-ZrP loading, the POST-ZrPn nanocomposites' T_g values increased at the beginning and then decreased slightly. The reason for this phenomenon can be attributed to the aggregation of α-ZrP nanoparticles. The incorporation of α-ZrP into PVA/OST blends also affected the melting temperatures. The T_m of POST-ZrP6 was ~ 22.3°C higher than that of POST-ZrP0; this was due to hydrogen bonding between α-ZrP and PVA/OST, which restricted the movement of molecular chains.

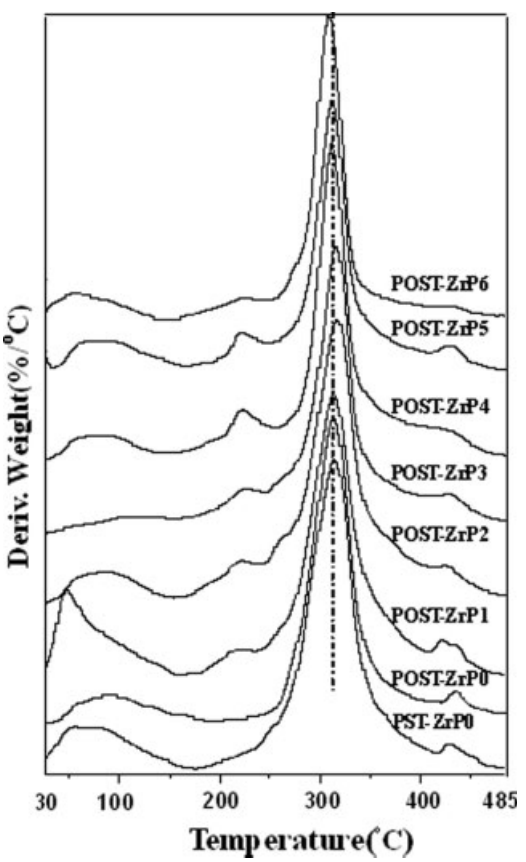

Figure 6 DTG curves for PST-ZrP0 and POST-ZrPn nanocomposite films with different α-ZrP contents.

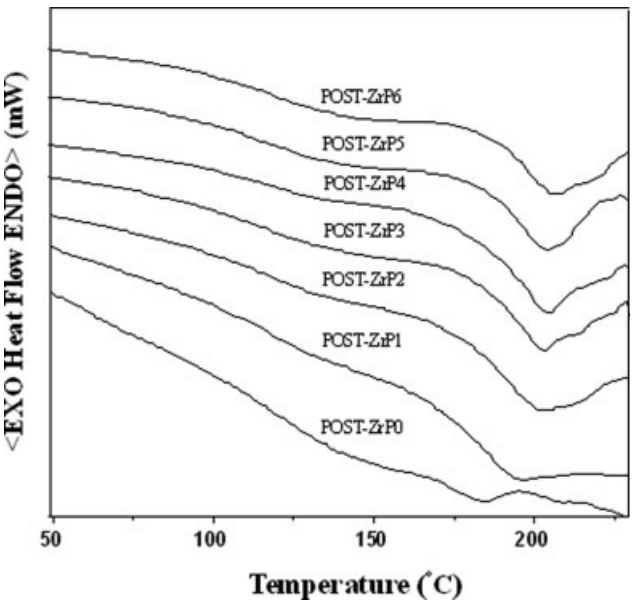

Figure 7 DSC curves for POST-ZrPn nanocomposite films with different α-ZrP contents.

The degradation temperatures, including IDT (initial decomposition temperature), T_{max} (temperature of the maximum rate of weight loss), FDT (final decomposition temperature), and IPDT (integral procedural decomposition temperature)[33] (Table II) were used to assess a material's stability. Comparing POST-ZrP0 with PST-ZrP0, T_m showed no difference, but both the IDT and FDT for POST-ZrP0 shifted to a higher temperature. This result indicates stronger hydrogen bonding between OST and PVA, which improves the thermal stability of POST-ZrP0. The degradation temperatures, including IDT, FDT, T_{max}, and IPDT, increased with the increased α-ZrP loading (≤1.5%) in POST-ZrPn. The improved thermal stability resulted from the reduced mobility of OST and PVA chains in the nanocomposites. Because of the interaction between polymers and nanofillers, the chain transfer reactions were suppressed; consequently, the degradation process was slowed, and decomposition took place at a higher temperature.[34] Higher levels of α-ZrP loading (≥2%) resulted in aggregations of α-ZrP particles and deterioration in film thermal properties. Results from MU and mechanical properties experiments confirmed this trend.

Mechanical properties

To illustrate the effect of the carboxyl groups in POST on the mechanical properties of POST-ZrPn, corresponding data for PST-ZrPn were used as controls. The mechanical properties of the blends (PST-ZrPn and POST-ZrPn series) are shown in Figures 8 and 9. In the PST-ZrPn nanocomposite films, when the α-ZrP loading was 1.5 wt %, σ_b and ε_b simultaneously reached a maximum of 8.0 MPa and 66%. The obvious improvement in σ_b and ε_b for such extremely low α-ZrP filler concentrations may be attributed to the following factors: First, permeation required for the small-size effect and the quantum tunneling effect of α-ZrP occurred. It was, therefore, easier to insert α-ZrP into polymer chains and destroy the ordered structure. Second, there may have been plenty of intermolecular hydrogen bonds that formed between α-ZrP and PVA/ST, which increased the miscibility and greatly improved the mechanical properties of the films. However, with higher α-ZrP content (≥2% wt %), both the tensile strength and elongation at break were sharply reduced. The reason for this may be aggregation of the nano-sized particles.

TABLE II
Thermal Analyses of PST-ZrP0 and POST-ZrPn Nanocomposite Films Measured by TGA and DSC

	Thermal analyses					
Sample	IDT (°C)	T_{max} (°C)	FDT (°C)	IPDT (°C)	T_g (°C)	T_m (°C)
PST-ZrP0	209.3	314.4	396.4	274.7	–	–
POST-ZrP0	243.4	314.8	403.6	276.4	111.2	186.2
POST-ZrP1	243.4	316.8	407.4	283.1	119.3	197.3
POST-ZrP2	246.5	318.2	409.9	304.6	120.9	203.7
POST-ZrP3	250.3	319.3	413.7	328.3	121.8	204.4
POST-ZrP4	260.4	312.8	408.0	252.0	119.8	205.8
POST-ZrP5	256.0	312.7	407.3	239.3	115.1	205.9
POST-ZrP6	254.1	310.6	406.7	230.1	113.6	208.5

IDT, initial decomposition temperature.
T_{max}, temperature of the maximum rate of weight loss.
FDT, final decomposition temperature.
IPDT, integral procedural decomposition temperature.
T_g, glass transition temperature.
T_m, melting temperature.

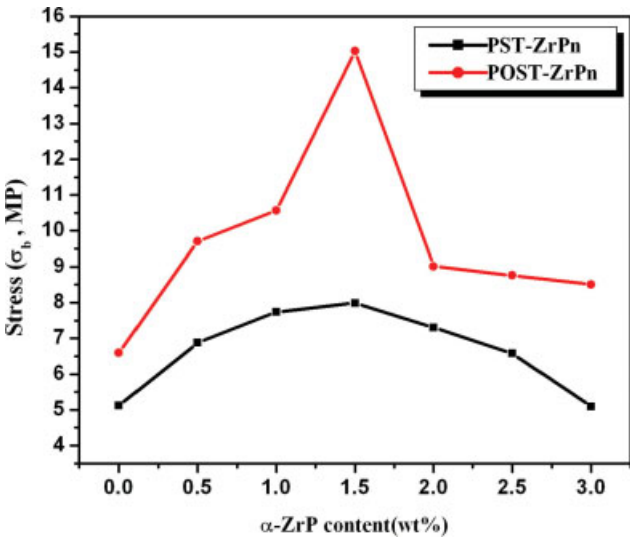

Figure 8 Tensile strength of PST-ZrPn, POST-ZrPn nanocomposite films with different α-ZrP contents. [Color figure can be viewed in the online issue, which is available at www.interscience.wiley.com.]

The POST-ZrPn series blends had the same tendency as PST-ZrPn. The σ_b and ε_b achieved a maximum of 15.1 MPa and 53% when the α-ZrP loading was 1.5 wt %. Mechanical properties of POST-ZrPn showed that σ_b was obviously higher, compared with PST-ZrPn at the same α-ZrP content, while ε_b was lower.

Moisture uptake

Moisture absorption is an important factor when dealing with hydrophilic thermoplastics because high water uptake worsens the mechanical properties of the material. One of the objectives of this work was to clarify the influence of oxidation on starch moisture absorption. To study this point, samples with and without oxidation were exposed to high humidity and the MU was determined gravimetrically. The results of this experiment are summarized in Figure 10, which shows the variation in MU with increasing α-ZrP content. The POST-ZrPn films had lower moisture absorption than PST-ZrPn films for all α-ZrP levels, indicating that the carboxyl groups formed a stronger network in the OST matrix and decreased the free volume of the polymers. When the α-ZrP was loaded, moisture absorption in both series was reduced, suggesting that α-ZrP had an interactive effect with the polymer matrix forming new hydrogen bonds and diminishing the number of —OH groups available for interaction with migrating water molecules. When the α-ZrP content was higher than 1.5 wt %, the MU increased as α-ZrP content increased but did not surpass the POST-ZrP0 (PST-ZrP0) level. The reason for this may be the aggregation of α-ZrP particles and the deterioration of film properties. This tendency suggested that the presence of α-ZrP decreased the MU and improved water resistance of the nanocomposite films.

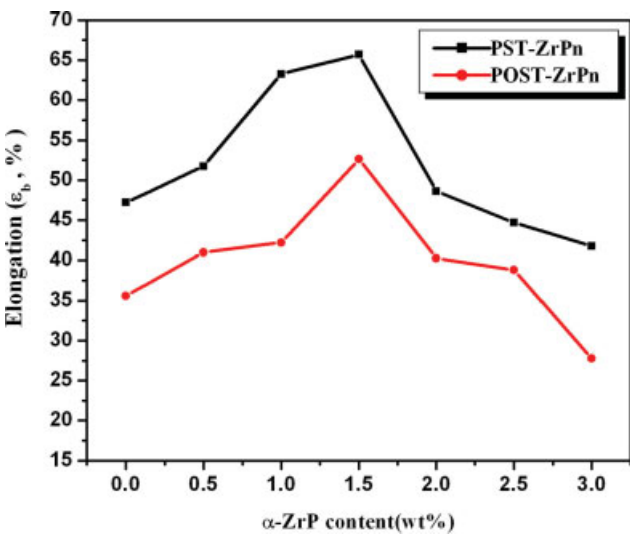

Figure 9 Elongation at break of PST-ZrPn, POST-ZrPn nanocomposite films with different α-ZrP contents. [Color figure can be viewed in the online issue, which is available at www.interscience.wiley.com.]

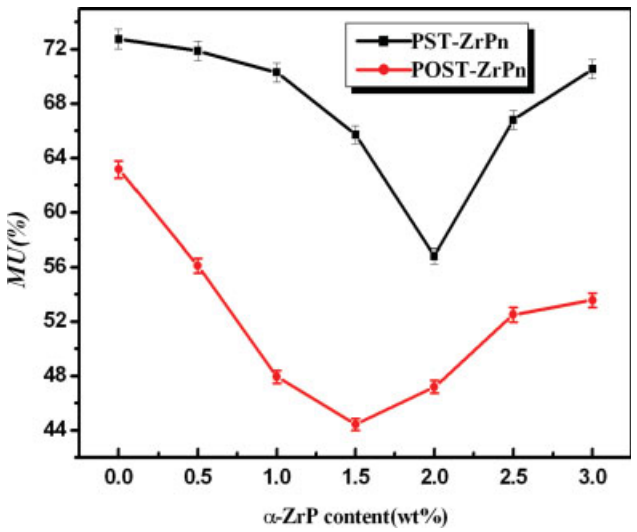

Figure 10 MU at equilibrium of PST-ZrPn and POST-ZrPn nanocomposite films with different α-ZrP contents. [Color figure can be viewed in the online issue, which is available at www.interscience.wiley.com.]

CONCLUSIONS

Two series of nanocomposite films (POST-ZrPn and PST-ZrPn) were prepared by a solution casting method. The results from FT-IR, XRD, and SEM indicated that the films of POST-ZrPn possessed better miscibility than PST-ZrPn, which resulted in improved mechanical properties and water-

resistance. Tensile strength and elongation at break of the POST-ZrPn nanocomposite films increased from 6.6 to 15.1 MPa and from 35% to 53% as the α-ZrP content increased from 0 to 1.5 wt %. Higher loading levels of α-ZrP resulted in aggregations of α-ZrP and deterioration of σ_b and ε_b. The presence of α-ZrP also decreased the MU and increased the degradation temperatures of the nanocomposites. The improvement in the properties of the POST-ZrPn nanocomposite films may have resulted from the formation of synergistic interactions and hydrogen bonding between α-ZrP and polymers.

References

1. Chakraborty, S.; Sahoo, B.; Teraoko, I.; Miller, L. M.; Gross, R. A. Macromolecules 2005, 38, 61.
2. Guan, J.; Hanna, M. A. Ind Eng Chem Res 2005, 44, 3106.
3. Dust, J. M.; Gajda, A. M.; Flickinger, E. A.; Berkhalter, T. M.; Merchen, N. R.; Fahey, G. C. J Agric Food Chem 2004, 52, 2989.
4. Spiridon, I.; Popescu, M. C.; Bodârlău, R.; Vasile, C. Polym Degrad Stab 2008, 93, 1884.
5. Martin, O.; Schwach, E.; Avérous, L.; Courturier, Y. Starch-Stärke 2001, 53, 372.
6. Chen, Y.; Cao, X. D.; Chang, P. R.; Huneault, M. A. Carbohydr Polym 2008, 73, 8.
7. Angellier, H.; Molina-Boisseau, S.; Dufresne, A. Macromolecules 2005, 38, 9161.
8. Cinelli, P.; Chiellini, E.; Lawton, J. W.; Imam, S. H. Polym Degrad Stab 2006, 91, 1147.
9. Zhao, G. H.; Liu, Y.; Fang, C. L.; Zhang, M.; Zhou, C. Q.; Chen, Z. D. Polym Degrad Stab 2006, 91, 703.
10. Dubief, D.; Samain, E.; Dufresne, A. Macromolecules 1999, 32, 5765.
11. Khan, M. A.; Bhattacharia, S. K.; Kader, M. A.; Bahari, K. Carbohydr Polym 2006, 63, 500.
12. Yoon, S. Y.; Deng, Y. L. Ind Eng Chem Res 2007, 46, 4883.
13. Lee, S. Y.; Chen, H.; Hanna, M. A. Ind Crops Prod 2008, 28, 95.
14. Giannakas, A.; Spanos, C. G.; Kourkoumelis, N.; Vaimakis, A.; Ladavos, A. Eur Polym J 2008, 44, 3915.
15. Magalhães, N. F.; Andrade, C. T. Carbohydr Polym 2009, 75, 712.
16. Sun, L.; Boo, W. J.; Browning, R. L.; Sue, H.-J.; Clearfield, A. Chem Mater 2005, 17, 5606.
17. Sun, L. Y.; Boo, W. J.; Sue, H.-J.; Clearfield, A. New J Chem 2007, 31, 39.
18. Sue, H.-J.; Gam, K. T.; Bestaoui, N.; Spurr, N.; Clearfield, A. Chem Mater 2004, 16, 242.
19. Yang, Y. J.; Liu, C. H.; Wu, H. X. Polym Test 2009, 28, 371.
20. Wu, H. X.; Liu, C. H.; Chen, J.; Chang, P. R.; Chen, Y.; Anderson, D. P. Carbohydr Polym 2009, 77, 358.
21. Huang, T. G.; Jiang, Q. M.; Zhang, B. L. Henan Chem Ind 2006, 11, 26.
22. Chattopadhyay, S.; Singhal, R. S.; Kulkarni, P. R. Carbohydr Polym 1997, 34, 203.
23. Trobajo, C.; Khainakov, S. A.; Espina, A.; García, J. R. Chem Mater 2000, 12, 1787.
24. Bermudez, R. A.; Colon, Y.; Tejada, G. A.; Colon, J. L. Langmuir 2005, 21, 890.
25. Mathew, S. H.; Brahmakumar, M.; Abraham, T. E. Biopolymers 2006, 82, 176.
26. Tang, S. W.; Zou, P.; Xiong, H. G.; Tang, H. L. Carbohydr Polym 2008, 72, 521.
27. Li, J. H.; Vasanthan, T. Food Res Intern 2003, 36, 381.
28. Ha, B.; Char, K.; Jeon, H. S. J Phys Chem B 2005, 109, 24434.
29. Yoshimura, M.; Takaya, T.; Nishinari, K. Carbohydr Polym 1998, 35, 71.
30. El-Khodary, A.; Oraby, A. H.; Abdelnaby, M. M. J Magn Magn Mater 2008, 320, 1739.
31. Qian, X. F.; Yin, J.; Huang, J. C.; Yang, Y. F.; Guo, X. X.; Zhu, Z. K. Mater Chem Phys 2001, 68, 95.
32. Jia, X.; Li, Y. F.; Zhang, B.; Cheng, Q.; Zhang, S. J. Mater Res Bull 2008, 43, 611.
33. Park, S. J.; Kim, H. C. J Polym Sci Part B: Polym Phys 2001, 39, 121.
34. Kuljanin, J.; Čomor, M. I.; Djoković, V.; Nedeljković, J. M. Mater Chem Phys 2006, 95, 67.